JOURNAL OF GEOPHYSICAL RESEARCH, VOL. 113, D08303, doi:10.1029/2007JD009104, 2008

Simulation of the evolution of aircraft exhaust plumes including detailed chemistry and segregation

A. Garmory,[1] R. E. Britter,[1] and E. Mastorakos[1]

Received 28 June 2007; revised 22 August 2007; accepted 19 December 2007; published 22 April 2008.

[1] The Field Monte Carlo or Stochastic Fields (SF) method for turbulent reacting flows has been applied to the chemical evolution of the early part of a hot jet with bypass flow producing 7kN of thrust, using a 23 species chemical mechanism. This is done to broadly approximate a turbofan engine at idle thrust setting. Much of the chemistry was found to take place inside the core of the jet before mixing occurs, as there is no reactant gradient there, considering segregation makes little difference. Radical concentrations, however, were found to be changed. The reaction between *NO* and ambient O_3, which is slow compared to the fast mixing timescale of the turbulent jet, is unaffected by segregation. The local Damköhler number was calculated based on an estimate of the chemical timescale and the local large-eddy timescale. It was found that only those species which had local *Da* greater than five were affected by segregation. In this work we have applied the SF method the early part of the plume, however the method developed here could equally be employed to study the plume over a longer distance.

Citation: Garmory, A., R. E. Britter, and E. Mastorakos (2008), Simulation of the evolution of aircraft exhaust plumes including detailed chemistry and segregation, *J. Geophys. Res.*, *113*, D08303, doi:10.1029/2007JD009104.

1. Introduction

[2] Given the rise in commercial air travel in recent times, the levels of pollution that people living or working near airports are actually exposed to has become increasingly important [*Department for Transport*, 2003]. This is currently even more important as future designs of jet engines will have to compromise between higher efficiencies and reduced NO_x emissions [*Greener By Design*, 2005]. In order to calculate correctly the levels of pollution the chemistry of individual plumes needs to be considered rather than just long term average concentrations. The large amounts of pollutants such as NO_x in the jet exhaust mean that even a considerable distance away from the aircraft the concentration in the plume will be much greater than an averaged background value. Some practical studies have been conducted to measure these levels such as by *Herndon et al.* [2004] who measured *NO*, NO_2, and CO_2 downwind of a runway at JFK airport and matched peaks with individual aircraft. Predicting computationally these levels is complicated by the turbulent nature of the flow and the reactions taking place destroying the primary pollutants and producing other, secondary, species.

[3] Studies have been performed on the chemical evolution of jet plumes at altitude, some of these [*Lewellen and Lewellen*, 2001] concern the region where the plume interacts with the wake vortices. However, much of the production of these secondary pollutants will take place close to the jet exhaust. The extent of this production will be controlled by the conditions in the jet itself and as such an insight into the effect of the jet on the chemistry will be of use. Whereas the wake vortex region at altitude will have a different composition and temperature from sea level, conditions in the early jet are set by the engine and so may be compared. *Kärcher et al.* [1996] have performed calculations of this early jet regime (1–2 km) for an aircraft cruising at altitude using a reaction mechanism with 23 species and 65 reactions. They calculate the flow field on an axisymmetric grid and use the velocity and temperature field from this at each step to calculate the transport of the scalars. The chemical kinetics are calculated in a separate operator-splitting stage at each step. The key chemical processes they studied were the transformation of *NO* to NO_2 and primary NO_x and SO_2 pollutants into nitrous, nitric and sulphuric acid, along with the evolution of radicals within the plume. The transformation of *NO* to NO_2 is of particular importance because, while it is primarily *NO* that is emitted in the exhaust, it is NO_2 levels that are controlled by regulation. They found that much of the chemistry takes place very early in the jet before turbulent mixing has a significant effect. Sulphuric acid and its precursor SO_3 play an important part in the generation of aerosols in the jet plume both directly and through interaction with carbon particles. This is discussed by *Brown et al.* [1996], who also found that condensation occurs closer to the exhaust nozzle when there is a bypass duct compared to a single jet for a High Speed Civil Transport (HSCT) aircraft on account of the mixing due to the bypass being more rapid compared to the axial velocity.

[1]Department of Engineering, University of Cambridge, Cambridge, UK.

0148-0227/08/2007JD009104$09.00

[4] The work discussed above does not include the full effect of the interaction of turbulence and chemistry. It does not include what are described as turbulent species correlation effects, which are sometimes known as segregation. In short, turbulence will create temporal and spatial fluctuations in reactant concentration, known as segregation, even at the smallest scales which will alter the mean reaction rate at that point. These fluctuations will decay due to the action of molecular mixing, which is also known as micromixing.

[5] We can further understand the micromixing problem by considering an expression for the mean reaction rate for a simple chemical reaction $A + B \rightarrow C$. The instantaneous reaction rate in a turbulent flow is given by $\dot{w} = \beta\phi_A\phi_B$, where ϕ the scalar concentration. If we perform a Reynolds decomposition and averaging we are left with:

$$\bar{\dot{w}} = k\left(\bar{\phi}_A\bar{\phi}_B + \overline{\phi'_A\phi'_B}\right) \quad (1)$$

The terms with overbars can be thought of as being a mean over a period of time or over a spatial area such as a grid cell. It can be seen that to calculate a mean reaction rate one must take account of the fluctuating terms $\overline{\phi'_A\phi'_B}$ and not just use mean reactant concentrations. In the above, we have neglected the effect of temperature for simplicity. In fact, if temperature fluctuations are considered then the difference from taking mean values only is even more pronounced due to the non-linear nature of the Arrhenius term.

[6] Common practice in much Air Quality Modeling has been to neglect the correlation term, partly due to the extra computational cost it requires. Whether this assumption is justified or not is dependent on the timescale of the reactions involved compared to the physical process destroying the correlation. The parameter that characterizes this is the Damköhler number, *Da*, which is the ratio of the physical timescale to a chemical timescale. The physical timescale will be that of the turbulence as it is this that controls the rate at which ϕ' is destroyed by the smallest eddies. A low value of *Da* indicates that the reaction is slow compared to the destruction of scalar fluctuations and therefore it is reasonable to neglect them. On the other hand a high *Da* indicates that the $\overline{\phi'_A\phi'_B}$ term may well have a significant effect. An effort to quantify the values of *Da* where this occurs is made in this paper. When the chemical mechanism is complicated it is possible that some reactions will be affected and others not. Further discussion of the influence of the relative sizes of mixing and chemical timescales on reaction rates in the context of atmospheric reactions are given by *Vinuesa and Vilà-Guerau de Arellano* [2003], *Galmarini et al.* [1995], *Jacobson* [1999], *Hilst* [2000], *Liang and Jacobson* [2000], *Brown and Bilger* [1998], and *Vilà-Guerau de Arellano et al.* [2004].

[7] Some attempts to take reactant correlation, or segregation effects, into account in the jet plume problem have been made. *Wang and Chen* [1997] made comparisons for a HSCT at Mach 2.4 between a box model technique assuming perfectly mixed reactants, a box model assuming imperfect micromixing (but perfect macromixing across the plume), a PDF simulation assuming perfect micromixing within a cell and a PDF simulation using the modified Curl's mixing model. Their conclusion was that using the PDF method without micromixing lead to about a 1% reduction in NO_x consumed by reaction compared to the box model approaches and that inclusion of Curl's model leads to a further 0.2% reduction.

[8] Another simulation of a HSCT plume has been made by *Menon and Wu* [1998] who use a linear-eddy model (LEM) to account for micromixing effects. This method uses a 1D grid with high enough resolution to resolve all length scales in the flow. This grid is marched downstream and expanded to account for large scale entrainment by assuming that the jet can be approximated by a round free jet. The turbulent mixing is represented by random mixing events whose position, timescale and lengthscale are chosen from appropriate distributions. Reaction-diffusion equations are then solved on the 1D grid. Using this method Menon and Wu show that NO_x consumption is reduced by a further 1% compared to *Wang and Chen* [1997]. It is evident from these simulations that segregation has a small impact on ozone and NO_x far downstream from the exhaust, but the extent to which this conclusion can be carried over to the region close to the source and to other species is not fully explored yet.

[9] In this work we employ the Field Monte Carlo method to a hot jet with a bypass flow using the chemistry of *Kärcher et al.* [1996]. The method is a PDF method and so gives information not just about mean values but also higher moments such as variances. It has been used for combustion problems, which are high *Da* reacting flows [*Mustata et al.*, 2006; *Sabel'nikov and Soulard*, 2006]. It has also been used to successfully simulate a laboratory turbulent plume with simple NO_x chemistry [*Garmory et al.*, 2006]. This showed that the Stochastic Fields method can be used to produce more accurate results in the context of atmospheric reacting flows. The conditions in our jet were chosen to give a thrust approximately equal to that of a 100 kN rated engine at idle thrust on the ground. It is not the purpose of this work to produce an accurate simulation of a particular jet plume. Rather, the objectives are: (1) to develop a Field Monte Carlo code coupled with a CFD solver that can readily be applied to practical problems. (2) To investigate the effects of segregation on the chemical evolution of a jet in its very early stages using a realistic chemistry.

[10] The structure of this paper is as follows; in section 2 we discuss the formulation of the Field Monte Carlo method and its implementation using existing CFD software. Section 3 describes the model problem investigated in this work including the CFD simulation of the flow field. The results with discussion are contained in section 4 followed by a summary of the conclusions.

2. Formulation

2.1. Field Monte Carlo Method

[11] The Field Monte Carlo or Stochastic Fields method is an Eulerian Probability Density Function (PDF) method developed by *Valiño* [1998] and later independently by *Sabel'nikov and Soulard* [2005]. Starting from the modeled one-point joint scalar PDF transport equation, equation (2), stochastic partial differential equations (spde's) are derived to govern the evolution of a number of fields which extend over the spatial domain of the flow. Each field contains values for each scalar at every point in the domain and the PDF at any single point is then represented by the ensemble

of scalar values at that point across all fields. This is distinct from Lagrangian PDF methods in which the PDF is represented by values attached to notional particles that move within the flow. The Field Monte Carlo method has similarities with two earlier stochastic methods for simulating flow, namely the CONNFFESSIT method used in *Laso and Öttinger* [1993] and also Spalding's multifluid method which was applied to turbulent combustion [*Spalding*, 1995].

[12] Valiño's derivation starts with the modeled joint scalar PDF transport equation, equation (2), using a gradient approximation with a turbulent diffusivity K for the conditional velocity fluctuation term. A closure is also needed for the molecular diffusion term, which in this case is modeled by the Interaction by Exchange with the Mean (IEM) using a timescale T_{eddy} [*Dopazo*, 1975]. The final modeled PDF equation is

$$\frac{\partial f_\phi}{\partial t} + u_k \frac{\partial f_\phi}{\partial x_k} - \frac{1}{\langle\rho\rangle}\frac{\partial}{\partial x_k}\left(\langle\rho\rangle K \frac{\partial f_\phi}{\partial x_k}\right) = -\frac{\partial}{\partial \psi_i}\left[\frac{\psi_i - \bar{\phi}_i}{T_{eddy}}\right] - \frac{\partial}{\partial \psi_i}\left[\dot{w}_i(\boldsymbol{\psi}) f_\phi\right] \quad (2)$$

where u_k is the mean velocity, ρ is the density and $\dot{w}_i(\boldsymbol{\psi})$ is the instantaneous reaction rate given composition ψ. The PDF is then represented by N stochastic fields defined as $f_\phi(\psi; \mathbf{x}, t) = \frac{1}{N}\sum_{n=1}^{N} \delta[\psi - \tau^n(\mathbf{x}, t)]$. These fields are defined by Valiño as being twice differentiable in space. Using this definition, and applying the chain rule, equation (2) is transformed into a pde in terms of ψ only (see *Valiño* [1998] for details). This is a Fokker-Planck equation describing the evolution of the Eulerian composition PDF. As such it has an equivalent stochastic pde [*Gardiner*, 2004] describing the evolution of the N stochastic fields representing f_ϕ. When interpreted in an Ito sense [*Gardiner*, 2004] this spde takes the form:

$$d\tau_i^n = -\bar{u}_k \frac{\partial \tau_i^n}{\partial x_k} dt + \frac{1}{\langle\rho\rangle}\frac{\partial}{\partial x_k}\left(\langle\rho\rangle K \frac{\partial \tau_i^n}{\partial x_k}\right) dt + \dot{w}\left(\tau_1^n, \tau_2^n, \ldots, \tau_N^n\right) dt + (2K)^{1/2} \frac{\partial \tau_i^n}{\partial x_k} dW_k^n - \frac{\tau_i^n - \bar{\phi}_i}{T_{eddy}} dt \quad (3)$$

where τ_i^n is the concentration of species i in field n and $\bar{\phi}_i$ is the mean concentration of the scalar, calculated as an average over the fields. dW_k^n is the increment of a Wiener process, i.e., a random process with zero mean and variance equal to the time elapsed [*Gardiner*, 2004]. Note that no two-point information may be inferred from the stochastic fields as the derivation starts with the single point transport equation.

[13] For more details about the Stochastic Fields method the reader is referred to *Valiño* [1998], *Sabel'nikov and Soulard* [2005] and *Garmory et al.* [2006], but a few points are worth noting again here. A turbulent diffusivity, K, is used due to an assumption in the original PDF transport equation that the turbulent conditional flux term can be modeled using a gradient hypothesis, and appears in both Valiño and Sabel'nikov's derivations. The final term on the right hand side of equation (3) represents the rate at which scalar fluctuations decay toward their mean values, i.e., micromixing. The model used here is the IEM model where the decay timescale, T_{eddy}, is here assumed to be the same as the turbulent velocity timescale. This is used as it is the timescale of the large scales of turbulence which determines the rate at which fluctuations in scalar quantities are passed down to the smallest scales where they are destroyed by molecular diffusion [*Jones and Kakhi*, 1998]. We have previously found this to produce mean and RMS values in excellent agreement with experimental data for passive scalars [*Garmory et al.*, 2006]. However, there is some evidence that this might not be accurate for reactive scalars [*Cha and Trouillet*, 2003], but more complex methods will have increased computational cost and require more fields for statistical accuracy.

[14] The fourth term is the random or 'Wiener' term, which can be thought of as representing random motions within the flow caused by turbulence. The strength of this term in producing scalar fluctuations will depend on the local turbulence level through K and the local scalar gradient. The chemistry term evaluates the reaction rate for each scalar using the scalars from that field and in this way the effect of fluctuations from the mean on the reaction rate are considered directly. As this method is a joint-scalar PDF method and not a joint-velocity-scalar PDF method information about the flow field must be provided via u_k, K and T_{eddy} for each spatial node, either from measurement or by modeling. In the context of RANS based CFD these quantities will represent an averaged value at each spatial location. The simulation produced by the Stochastic Fields method will therefore depend directly on the flow field data and hence on the method used to obtain it.

[15] *Sabel'nikov and Soulard* [2005] derive governing equations for the stochastic fields in a different way. They do this by writing an spde with an advection term split into a deterministic part and a Gaussian random part. The form of these parts are then chosen so that the spde is stochastically equivalent to equation (2). They state that the random advection term must preserve the correct properties of advection, that is it must not introduce diffusion into an individual field. In order to preserve this property the random term of the spde is implemented using Stratonovich calculus, in which the coefficient of the random term is evaluated at the mid point of the timestep, rather than the beginning as in Ito calculus *Gardiner* [2004]. The spde so derived is:

$$d\tau_i^n = \left[\left(-u_k + \frac{1}{2}\frac{\partial K}{\partial x_k} + \frac{K}{\langle\rho\rangle}\frac{\partial\langle\rho\rangle}{\partial x_k}\right)\frac{\partial \tau_i^n}{\partial x_k} - \frac{\tau_i^n - \bar{\phi}_i}{T_{eddy}} + \dot{w}\left(\tau_1^n, \ldots, \tau_N^n\right)\right] dt + \sqrt{2K}\frac{\partial \tau_i^n}{\partial x_k} \circ dW_k \quad (4)$$

where $\circ$ implies that the integral is to be performed in the Stratonovich sense. Again the IEM model is chosen as the closure for the molecular diffusion term, although the spde has been derived without any particular closure being specified. It can be shown that this spde is equivalent to equation (3). *Gardiner* [2004] shows that a Stratonovich spde of the form

$$dx = a dt + b \circ dW \quad (5)$$

is the same as the Ito spde

$$dx = \left[a + \frac{1}{2} b \frac{\partial b}{\partial x}\right] dt + b dW \tag{6}$$

[16] It can easily be shown that if equation (4) is compared to equations (5) and (6) then the term

$$\frac{\partial}{\partial x_k}\left(K \frac{\partial \tau_i^n}{\partial x_k}\right) - \frac{1}{2} \frac{\partial K}{\partial x_k} \frac{\partial \tau_i^n}{\partial x_k} \tag{7}$$

must be added to the deterministic part of equation (4) to convert to Ito calculus. If this is done we are left with equation (3), showing that the two spde's are mathematically equivalent provided they are interpreted in the correct sense. Because of this it is possible to use Sabel'nikov's less restrictive derivation (which places no constraint on the differentiability of the stochastic fields) to derive Valiño's Ito spde. The numerical implementation of the method is unaffected by the details of the derivation.

[17] We have found the Ito method, equation (3), to be the more easily implemented as the Stratonovich implementation was prone to instability due to the absence of a second spatial derivative term. Equation (3) is also more suitable when coupled with an existing CFD code, which can be used to calculate the advection and diffusion terms as described below in section 2.2. Owing to this we have chosen to use the Ito method. Finally, it should be noted that if the final two terms of equation (3) are neglected and only one field is used then we are left with a simple advection-diffusion-reaction model, without any segregation effects, which can be used for comparison to highlight the effects of micromixing on the calculation.

2.2. Numerical Methods

[18] As stated above in section 2.1, the Stochastic Fields method requires information about the flow field at each point in the grid. In this case the information must be produced by a CFD simulation of the flow field. However, the first two terms of equation (3) represent an advection-diffusion system that can also be solved using an existing CFD package. As such we have implemented the Stochastic Fields method for this work by coupling it with a commercial CFD package, namely FLUENT Version 6.2.

[19] This has been done by using a fractional step method where advection-diffusion terms are solved first, then the Wiener or random term and finally the chemistry and micromixing terms. We make use of the User Defined Scalars (UDS) available in FLUENT, these are up to 50 arbitrary scalars, ϕ_i, for which FLUENT solves a transport equation:

$$\frac{\partial \rho \phi_i}{\partial t} + \frac{\partial}{\partial x_k}\left(\rho u_k \phi_i - \Gamma_i \frac{\partial \phi_i}{\partial x_k}\right) = S_{\phi_i} \quad i = 1, \ldots, N \tag{8}$$

[20] This equation is solved by an iterative, implicit method, which should ensure the stability of the advection-diffusion scheme. If we set the source term $S_{\phi i}$ to zero and set $\Gamma_i = \rho K$ then FLUENT will solve the first advection-diffusion fractional step for each scalar in each field as required. We assume a turbulent Schmidt number of unity and thereby set ρK equal to the effective dynamic viscosity, which is calculated by FLUENT. The simulation is run as an unsteady case, so the advection-diffusion is solved for all scalars for one timestep before a user defined subroutine, written by ourselves, is used to perform the remaining fractional steps and update the scalar values before the next timestep.

[21] The second fractional step is the random forcing term for which we use an Euler-Maruyama approximation of an Ito process, which converges with order 0.5 w.r.t. timestep in the path-wise sense but 1.0 in the average [*Kloeden and Platen*, 1999]. The increment of a Wiener process is given by $dW_z^n = \xi_z^n dt^{1/2}$ where ξ_z^n is a Gaussian random number with zero mean and unity variance. An independent value of ξ is required for each spatial component in each field. Within the same field scalars will have the same value for a given component. FLUENT provides the three Cartesian components of gradient for each scalar and hence the second fractional step can be calculated as

$$\begin{aligned}\tau_i^n(t + \Delta t) = {} & \tau_i^n(t^*) \\ & + (2K)^{1/2}\left[\frac{\partial \tau_i^n(t^*)}{\partial x}\xi_x^n \right. \\ & \left. + \frac{\partial \tau_i^n(t^*)}{\partial y}\xi_y^n + \frac{\partial \tau_i^n(t^*)}{\partial z}\xi_z^n\right](\Delta t)^{1/2}\end{aligned} \tag{9}$$

at each grid cell for each scalar i in every field n. K is found by dividing effective dynamic viscosity from the CFD by the density. As by *Garmory et al.* [2006] the maximum size of the Wiener step is limited to the difference between the current scalar value and it's upper or lower physical limit. This is done rather than bound the scalar after the step as this would lead to the term being biased toward values that move away from the limit. Equation (9) is an explicit Euler approximation to a stochastic advection process, which by itself would be unstable. To correctly calculate an Ito integral the integrand of the random term must be independent of ΔW [*Gardiner*, 2004], hence care should be taken when choosing the numerical method used to ensure that this is the case. We have found our method outlined above to be stable when used in this way with a separate advection-diffusion fractional step [*Garmory et al.*, 2006]. It has furthermore been found to agree with results obtained for a test-case using the equivalent Stratonovich spde equation (4) for which Runge-Kutta type methods can be used [*Sabel'nikov and Soulard*, 2005].

[22] One scalar in each field represents temperature and by applying equation (9) to this scalar the effect of fluctuations of temperature on the reaction rate is considered. The temperature is unaffected by the reaction of other scalars in this flow as the heat released by them is small and as such the mean temperature is unaffected, as is the flow field. This means that, for this flow, the CFD solution does not require information from the Stochastic Fields code and hence a steady state CFD solution can be used, i.e., one-way coupling.

[23] The final fractional step involves the chemistry and micromixing terms. This is performed for each grid cell in turn. The mean for each scalar is calculated first before the scalars, together with $T_{eddy} = k/\epsilon$, are used in equation (10) to evaluate the effect of chemistry and micromixing for each field at a time:

$$\frac{d\tau_i^n}{dt} = \dot{w}\left(\tau_1^n, \tau_2^n, \ldots, \tau_N^n\right) - \frac{\tau_i^n - \overline{\phi}_i}{T_{eddy}} \tag{10}$$

[24] The CHEMEQ2 stiff ODE solver [*Mott and Oran*, 2001] was used to solve equation (10). It is a predictor-corrector algorithm [*Oran and Boris*, 2001] which is described as an α-quasi-steady state method. CHEMEQ2 is a single point method requiring only information from the current time level, this makes it particularly suited to solving the chemistry across a grid in this fractional step method. The CHEMEQ2 solver was chosen after comparison with a backward multistep solver, VODPK [*Byrne*, 1992]. VODPK is capable of greater accuracy, but the need to build up historical data for each calculation leads to a start-up penalty. The two solvers were tested using a 0D calculation, whereby only chemistry was considered for random initial conditions, and in an advection-diffusion-reaction calculation. With adjustment of its solution parameters it was possible to get acceptable accuracy from CHEMEQ2 compared to VODPK for both these cases. CHEMEQ2 was found to be significantly faster. In order to place a check on the errors due to calculating the mean concentration $\bar{\phi}_i$ before equation (10) is solved we also calculated the micromixing term separately after the chemistry using the analytical solution to the IEM model.

[25] As the mechanism used in this work has 24 species (section 2.3) and FLUENT only allows for 50 UDS, it can be seen that this does not leave much scope for using many fields. However, the only term in which the fields influence one another is the micromixing term. As such, the first two fractional steps can be performed in batches of 2 fields or 48 scalars, while the other fields are stored in memory. After the first FLUENT timestep the user subroutine performs the second fractional step on the UDS before writing these scalars to memory and writing a new batch of scalars to the UDS. This is repeated until all scalars have undergone the first two steps. The chemistry and micromixing step is then performed on all scalars before the process starts again. Twelve fields have been used in this work and hence steps 1 and 2 are performed in 6 batches. It has been found that this swapping process takes very little time compared to the rest of the calculation and, as the flow solver can be switched off, this method is not significantly slower than calculating all fields simultaneously. Means and RMS values for each scalar can be calculated and stored in memory throughout the grid. These can then be processed using FLUENT's post-processing tools.

[26] As with all Monte Carlo calculations the standard deviation of the statistical error in calculating mean quantities from a sample of N realizations is, according to the central limit theorem [*Tennekes and Lumley*, 1972]:

$$E_s = \frac{\sigma}{\sqrt{N}} \tag{11}$$

where σ is the standard deviation, or rms, of the measured quantity. Hence as more fields are used the error will decrease as the inverse of the square root of the number of fields.

[27] There are several advantages to using an existing CFD package. A CFD solution has to be produced anyway to provide $\bar{u}$, K and T_{eddy} so it is clearly useful to use this same solution for the Stochastic Fields simulation, there is no need to produce a new grid and export flow field data from the CFD to the new grid. The treatment of advection and diffusion as well as boundary conditions is well developed in commercial CFD and hence there is no need for this to be repeated. It is also straightforward to switch between the different modeling options in the CFD, provided that $\bar{u}$, K and T_{eddy} can be found. The existing meshing and post-processing tools can be used making it simple to set up new problems and extract required data. Furthermore, parallelization with splitting the mesh between CPU's is then easily done. This is particularly efficient with this Stochastic Fields code as the expensive chemistry and micromixing terms require only local data, so that during this fractional step each CPU can run without incurring penalties due to the need to communicate with others.

2.3. Chemical Mechanism

[28] The size and complexity of the chemical mechanism that can be used with the Stochastic Fields method is limited only by the time and computing resources available. There must be a compromise between having enough fields for statistical accuracy, high enough spatial grid resolution and using a realistic mechanism. We have used 12 and 18 fields and the mechanism used here is taken from *Kärcher et al.* [1996]. It was developed to model the evolution of the first 2–3 km (or around 10s) of a jet engine plume. It has 24 scalars (including temperature) and 65 reactions. It does not include any hydrocarbon chemistry as their reactions take place on a timescale of minutes, too long to affect conditions in our period of interest. This was confirmed in preliminary work undertaken with an alternative mechanism taken from *Treviño and Méndez* [1999]. This 13 species ozone chemistry includes NO_x and CH_2O. The latter affects the chemistry through photolysis reactions which have timescales longer than our period of interest.

3. Model Problem

3.1. Jet Plume Flow Field

[29] In this section we discuss the CFD simulation of the jet plume and the conditions in the jet and its surroundings. A simplified geometry is used to represent the rear of a jet engine, it consists of a 0.48 m diameter core surrounded by an annular bypass of outer diameter 1.0 m. This geometry was incorporated into two grids. The first, known as Mesh 1, has the jet centrally positioned in a 10m diameter circular inlet plane. The mesh extends 50 m downstream with the diameter increasing to 60 m. There are 72 triangular faces on the core, 206 on the bypass and 1538 on the surrounding ambient air inlet where the meshing has the same spacing as the bypass close at the center becoming coarser toward the edge. The meshing is projected downstream with the cell sizes growing at the same rate as the overall diameter. The spacing in the downstream direction is initially 0.2m growing with a ratio of 1.112. The total number of grid cells is 50,848.

[30] Mesh 2 is a 5 × 5 × 10 m box with the jet center central in the horizontal direction and 2 m up in the vertical direction. It has 48 triangular faces on the core, 154 on the bypass and 956 on the surrounding ambient air inlet. The downstream spacing is 0.1 m initially growing to a maximum of 0.4 m with a ratio of 1.05, giving a total number of grid cells of 45,162. This mesh has greater resolution in the

jet axis direction to allow rapid chemical evolution close to the jet to be better observed.

[31] The flow field was computed prior to the reacting flow modeling as a steady state compressible flow by solving equations for continuity, energy and turbulence using the k-ϵ model [*Fox*, 2003]. The jet is assumed to be air. For inlets to the domain static pressure, p; total pressure, P_0 and total temperature, T_0 are specified along with turbulent kinetic energy k and turbulent dissipation rate, ϵ. For outlets from the domain p, T_0, k and ϵ are specified.

[32] The boundary conditions for the core and bypass have been chosen to give a total thrust of 7 kN. The conditions used were atmospheric pressure (101.325 kPa) for both core and bypass with gauge total pressures (above atmospheric) of 1.12 kPa for the bypass and 15.81 kPa for the core. Total temperatures were T_{0b} = 290 K and T_{0c} = 422 K, these conditions correspond to Mach numbers of $M_c = 0.46$ and $M_b = 0.13$. Hence the velocities at the engine exit plane were 186 ms^{-1} at the core and 43 ms^{-1} at the bypass. Static temperatures were 405 K in the core and 289 K in the bypass.

[33] The total pressure on the conical side boundary was set to be equal to ambient pressure while that on boundary surrounding the bypass was set to be 10Pa above ambient. The latter was done in order to aid convergence of the CFD solution. The ambient turbulence was set to be very low, with values of $k = 1.0 \times 10^{-3}$ m^2 s^{-2} and $\epsilon = 1.0 \times 10^{-4}$ m^2 s^{-3}. The turbulence in the jet at inlet was also set to relatively low values of $k = 1.0$ m^2 s^{-2} and $\epsilon = 1.0$ m^2 s^{-3}, however the results were found to be very insensitive to these parameters. It was found that the turbulence field observed in the plume is that produced by the shear layers between core and bypass and also bypass and ambient.

[34] Figure 1a shows a contour plot of mean velocity magnitude on a plane containing the jet axis for Mesh 1. Figure 1b depicts contours of radial velocity on a plane 10 m downstream of the exhaust, which shows the entrainment of ambient air into the jet. The key turbulence parameters for the Stochastic Fields method are K and T_{eddy}. Contours of ρK are shown in Figure 2a and T_{eddy} in Figure 2b. The very small turbulent timescale in the jet indicates rapid micromixing in this region. A CFD calculation was also performed using the same boundary conditions with the Reynolds Stress model, which gave very similar results. We will use the values of T_{eddy} later for calculating species Damköhler numbers.

[35] To ascertain whether Mesh 2 gives acceptable results it was used with the same conditions as described above in this section. It was found that there was good agreement for the velocity and turbulence field, indicating that the shorter distance to the side boundaries in Mesh 2 is acceptable. The finer spacing in Mesh 2 should also lead to better resolution for the jet in still air, particularly for the fast chemistry in the early plume.

3.2. Initial Compositions

[36] The background air chemical composition used in this work is shown in Table 1, together with volume fractions of the primary species at the exit plane of the engine core. Conditions in the bypass stream are assumed to be the same as the background. Background O_3, NO and NO_2 values were chosen to be representative of values at sea level in the United Kingdom, with these values 1.0×10^{-13} ppm was chosen for O as this was close to the equilibrium level. Other radical volume fractions have been set to the same values as those given by *Kärcher et al.* [1996], who suggest that these values are not crucial.

[37] For the conditions at the jet exit plane we again take the values from *Kärcher et al.* [1996], which should still be representative of a jet at ground level for all species other than NO, NO_2 and OH. The CO_2 level may be higher than in a real jet exhaust, but as an inert scalar in this mechanism it will not affect the chemistry. To estimate the NO_x volume fraction we have used data from the ICAO Emissions Data Bank for the IAE V2525-D5 engine *ICAO* [2004] (which has a thrust of 7kN at idle). This gives a fuel flow rate and Emission Index (EI) in g per kg for NO_x at idle thrust at sea level, from which a NO_x mass flow rate can be found. By using perfect gas relations for a compressible flow the total mass flow rate for the core can be found from the conditions at the core (section 3.1). This is found to be 29.3 kg s^{-1}. Volume fraction can then be found:

$$X_i = \frac{\overline{MW}_{air}}{MW_i} \frac{\dot{m}_i}{\dot{m}_{tot}} \tag{12}$$

[38] We chose to follow *Kärcher et al.* [1996] and make the NO_x at the exit plane 95% NO and 5% NO_2. The SO_2 level corresponds to an EI of 2.9g kg^{-1}, which is not far above the range expected from kerosene [*Kärcher et al.*, 1996]. For OH the emission index is uncertain so we chose to use a value that maintained the same proportion between NO_x and OH as found by *Kärcher et al.* [1996].

4. Results and Discussion

[39] For Mesh 1 both the plain advection-diffusion-reaction code and the Stochastic Fields code were used with a timestep of $\Delta T = 5.0 \times 10^{-4}$. For the Stochastic Fields code a total of 18 fields were used. The solution was found to be steady on average after about 6.0 s of simulated time. Results were taken for both codes after 8.0 s and 10.0 s of simulated time. The turbulent timescale in the plume is of the order of 10^{-2} s so taking further results at 2.0 s intervals is equivalent to using different random number sequences for results in the plume. Mesh 2 has a finer axial grid resolution and so both the Stochastic Fields code and the plain advection-diffusion-reaction code were used with a timestep of $\Delta t = 10^{-4}$ s. For Mesh 2 (section 3.1) it was found that the solution was steady on average by 0.5 s of simulated time. Mean results were taken at this point for the plain code and Stochastic Fields code. This was done for several runs with different random number sequences, 12 stochastic fields were used with Mesh 2. To run to a simulated time of 0.5 s using Mesh 2 the Stochastic Fields code took approximately 100 h when running in parallel on two Pentium 4, 3.0 GHz HT CPU's with 2 GB dual channel memory.

4.1. Inert Mixing

[40] CO_2 is unaffected by chemical reaction in this mechanism, and hence its chemical reaction rate is explicitly set to zero in the solver. Because of this it can be used to characterize the inert mixing of species in the plume. The

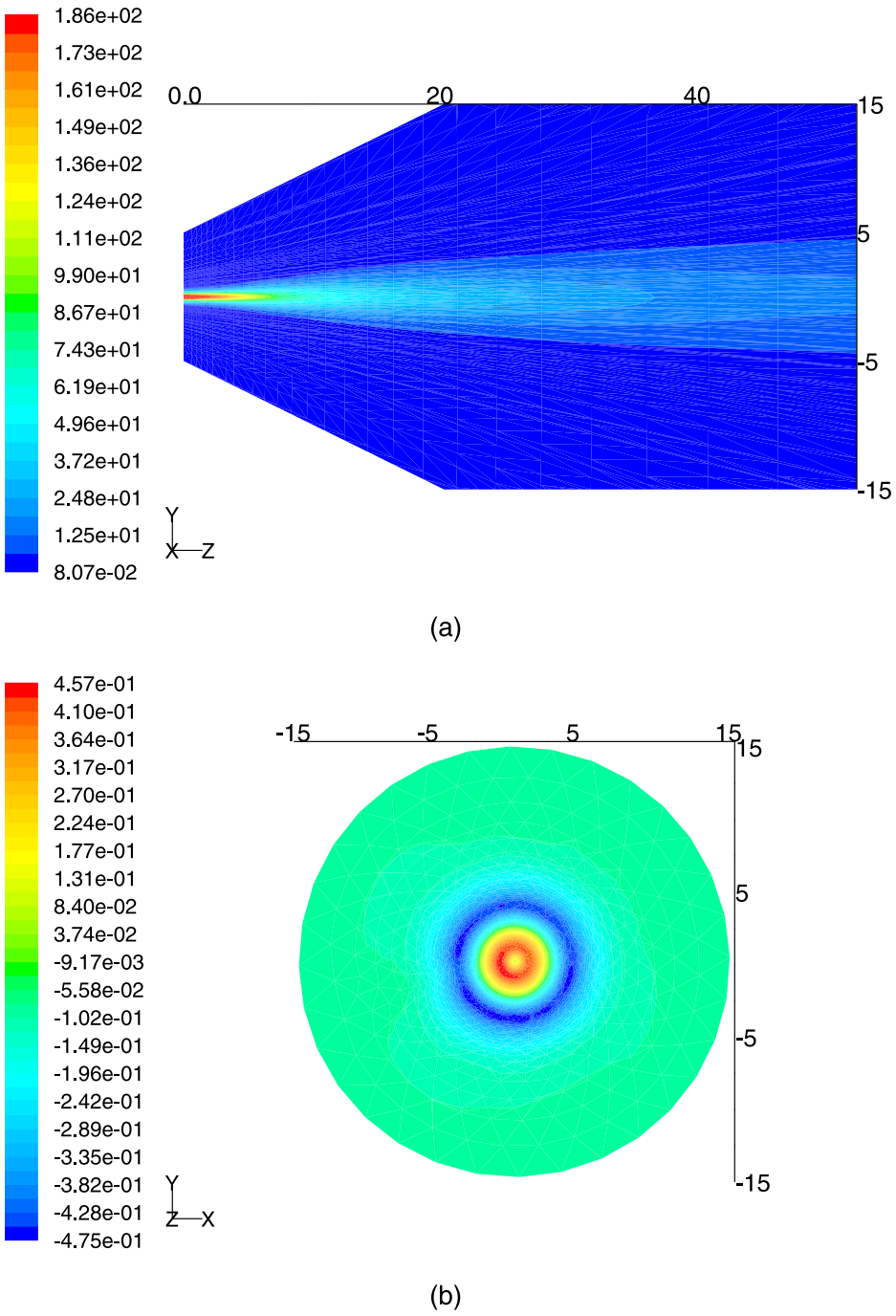

Figure 1. Contours of (a) velocity magnitude [m s^{-1}] for Mesh 1 on plane containing the jet axis, (b) radial velocity [m s^{-1}] on a plane perpendicular to jet axis 20 m downstream.

evolution of CO_2 along a line extending from the center of the jet is shown in Figure 3. Shown here is the volume fraction as calculated by both a simple advection-diffusion method, equation (8) (labeled "plain"), and by the Stochastic Fields method with 12 fields. There is an almost constant value in the potential core (about 4 core diameters) before rapid dilution when the turbulent mixing reaches the center of the jet. We also see that the RMS is zero before increasing sharply at this point, this is as expected as the scalar variance is caused by the gradients.

[41] In the absence of chemistry, terms 4 and 5 of equation (3) should not affect the first moment of the scalars. Therefore any difference between results for inert mixing by the S.F. method and by equation (8) must be due to statistical error. The agreement between the two lines on Figure 3 indicate an acceptable level of statistical accuracy in this calculation. This is also supported by the magnitude of the RMS values, which have a peak of 25% of the mean before falling to around 15% downstream, using equation (11) this corresponds to statistical errors with a peak value of

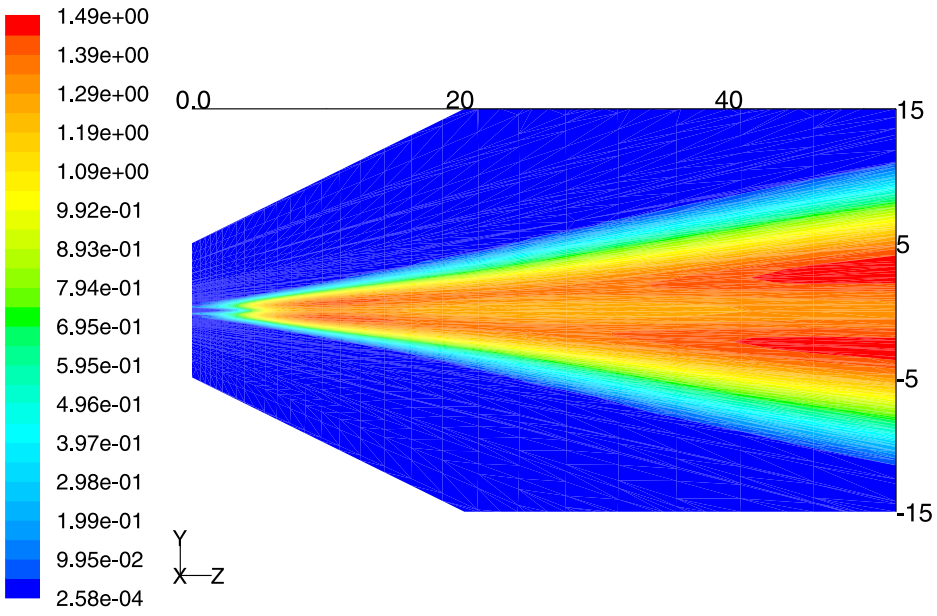

(a)

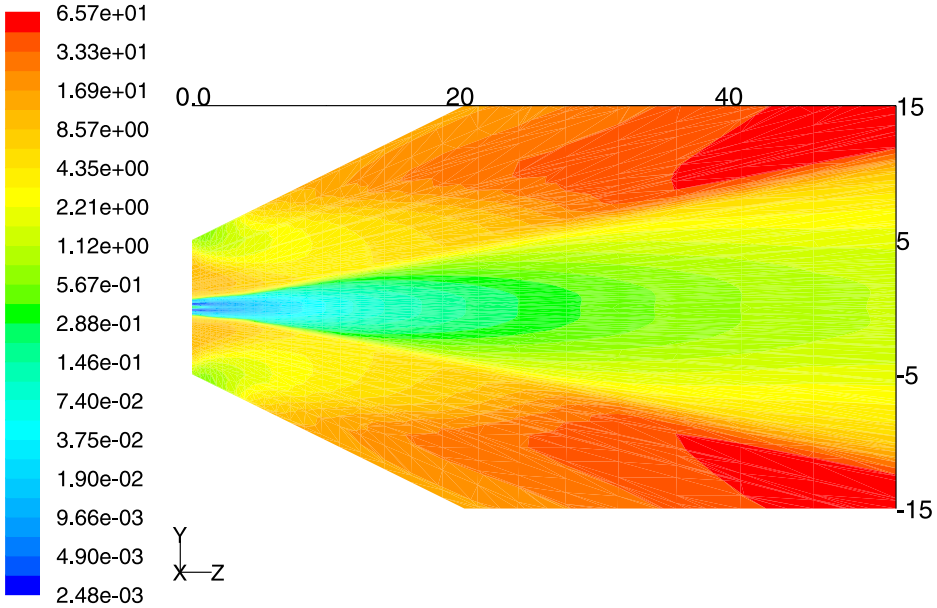

(b)

Figure 2. Contours of (a) turbulent viscosity, ρK, [kg m^{-1} s^{-1}] and (b) turbulence timescale, T_{eddy}, [s] for Mesh 1 on plane containing the jet axis.

6% of the mean, falling to 3.5% downstream, when 18 fields are used. If 12 fields were used the peak statistical error would increase only to 7.2%. It is worth noting that to reduce the peak error to 1% it would be necessary to use 625 fields, which is a prohibitatively high number.

[42] As CO_2 is an inert species here and its volume fraction in the background is negligible compared to its value in the jet we can use it to give a mixture fraction by normalizing using the jet core inlet value. *Richards and Pitts* [1993] give expressions for mean and RMS of mixture fraction ($\bar{\xi}$ and ξ') for the axisymmetric free jet. Along the axis of the jet these become:

$$\bar{\xi} = \left(\frac{\rho_{jet}}{\rho_{air}}\right)^{1/2} \frac{9.52 r_0}{z - z_{0Y}} \tag{13}$$

$$\xi' = \left(\frac{\rho_{jet}}{\rho_{air}}\right)^{1/2} \frac{2.19 r_0}{z - z_{0Y}} \tag{14}$$

Table 1. Jet Core Exhaust and Background Volume Fractions

Species	Core, ppm	Background, ppm
O	0	1.0×10^{-13}
O_2	1.35×10^5	2.1×10^5
O_3	0	3.86×10^{-2}
H	0	0
H_2	0	9.0×10^{-1}
OH	9.5×10^{-1}	2.8×10^{-7}
HO_2	0	3.6×10^{-6}
H_2O	3.6×10^4	8.8×10^1
H_2O_2	0	2.4×10^{-5}
NO	1.89×10^1	1.86×10^{-2}
NO_2	9.9×10^{-1}	3.14×10^{-2}
NO_3	0	8.9×10^{-9}
N_2O_5	0	1.0×10^{-5}
HNO_2	0	3.4×10^{-7}
HNO_3	0	2.0×10^{-3}
HNO_4	0	1.1×10^{-4}
CO	9.4×10^1	4.0×10^{-2}
CO_2	3.8×10^4	3.3×10^2
SO	0	0
SO_2	5.8	9.1×10^{-6}
SO_3	0	0
HSO_3	0	0
H_2SO_4	0	0

where r_0 is the jet nozzle radius and z_{0Y} is the virtual origin taken at 7.2 r_0. The presence of a co-flowing bypass jet means that this expression is not fully valid here but it may be used to give an approximation. Figure 4 shows the above expressions compared to our simulations. Equations (13) and (14) have been evaluated both by considering only the jet core, which has a radius of 0.24 m, and by assuming the jet radius to include the bypass (0.5 m) as well. We see that our data initially agrees with the data for r_0 = 0.24 m, but further downstream the bypass jet has an effect and the gradient of our data with downstream distance becomes closer to that of the larger jet radius case. We also see

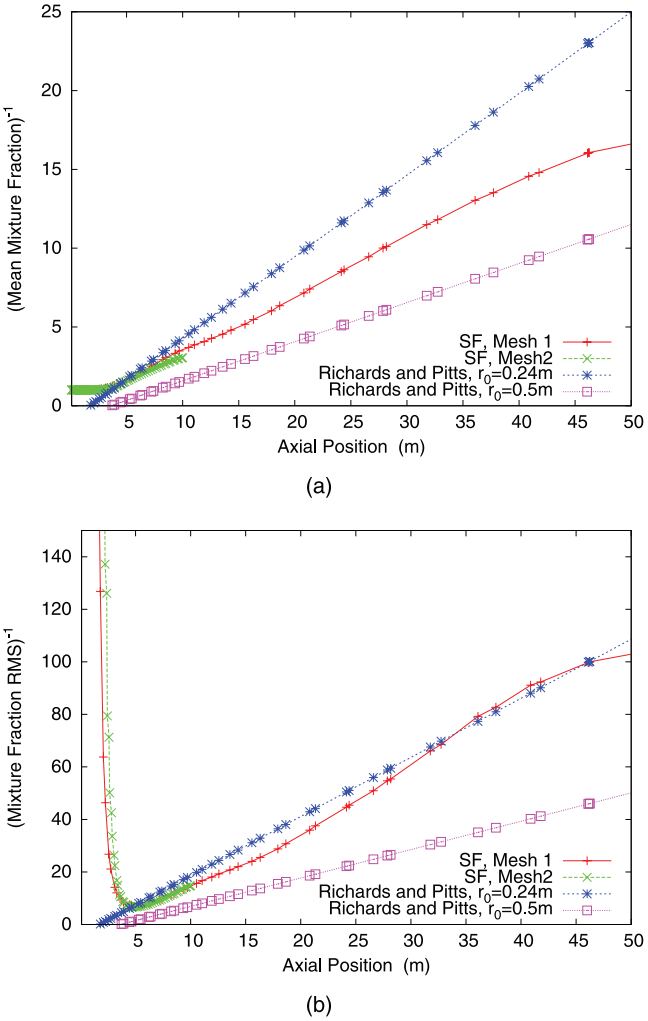

Figure 4. Mean (a) and RMS (b) of mixture fraction, ξ, along jet axis compared with the expression for mixture fraction from *Richards and Pitts* [1993].

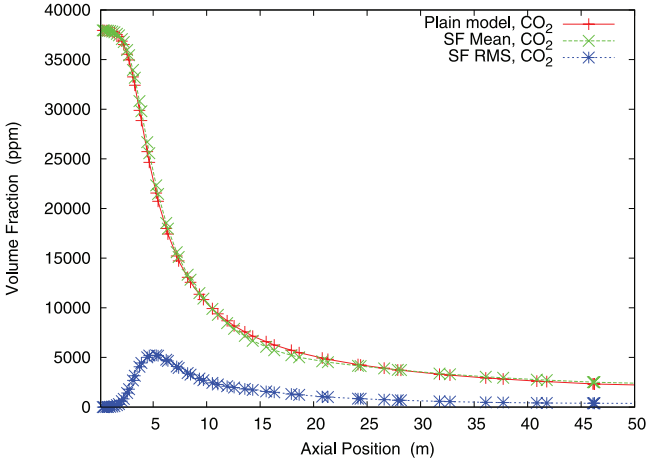

Figure 3. Evolution of CO_2 volume fraction in Mesh 1 along the jet axis downstream from jet exit plane. Results for the mean values using the full S.F. method and simple advection-diffusion are shown together with RMS values from S.F.

reasonable agreement between results using the 10 m and 50 m meshes.

4.2. Concentrations in the Reacting Plume

[43] First we will consider the progress of the primary pollutants in this mechanism, namely NO and NO_2, using Mesh 1. We can see in Figure 5a that in the first few meters NO_2 is produced within the plume. Figure 5b shows a corresponding reduction in NO, however due to the much greater concentration of this species in the plume the effect is less pronounced. Once the end of the jet core is reached these species are mixed out into the background. For NO in particular it can be seen that the profile in the reacting jet is very similar to that in an inert simulation. This is due to the high initial concentration in the jet, which means that the chemical effects caused by other more dilute species is small compared to turbulent mixing.

[44] In the jet core ozone, which was set to zero at the exit plane, is initially produced by the reaction $O + O_2 \rightarrow O_3$. The level produced is much lower than ambient levels, and a sharp increase is seen caused by the jet mixing out, Figure 5c. Further downstream into the mixing regime, the O_3

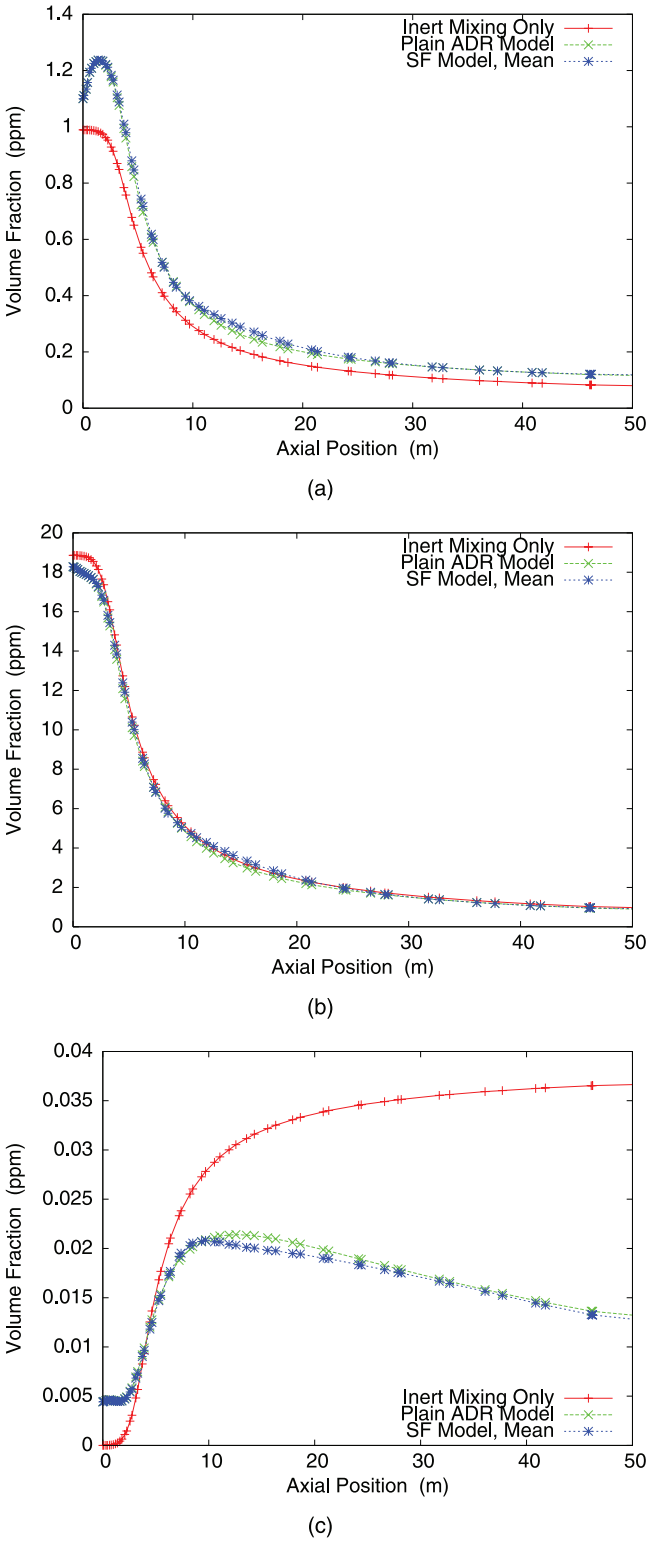

Figure 5. Axial evolution of the means of (a) NO_2, (b) NO and (c) O_3 along the center-line of jet into still air using Mesh 1. Calculations using inert mixing only, plain advection-diffusion-reaction model and Stochastic Fields model.

levels do not approach those in the background and in fact decrease. This is due to the very high level of NO in the plume which reacts with the O_3 by the reaction $NO + O_3 \rightarrow NO_2 + O_2$. The effect on NO and NO_2 is less obvious due to their high concentrations at this stage. In the presence of VOC's, NO_x will act to increase ozone levels overall, but this happens on a timescale considerably longer than the one we are considering. We see in Figure 5 that neglecting micromixing effects does not have a significant effect on predicted levels of these three pollutants. We have seen that the chemistry has little effect on NO_x compared to turbulent mixing, so we would not expect the effect of micromixing on chemistry to have a noticeable influence.

[45] We also see that for NO (and NO_2), see Figure 6a, the peak variance is located around the end of the jet core and that this peak is relatively distinct. If we compare it with O_3, Figure 6b, we see that there is also an area of high variance close to the end of the jet core, where large gradients are encountered due to mixing. However, unlike NO, we also observe another region of high variance further downstream, around 40–50 m from the jet. This is likely to be because the $NO + O_3 \rightarrow NO_2 + O_2$ reaction is reducing the O_3 concentration significantly compared to its effect on NO and NO_2. In this case the chemistry leads to larger gradients and hence variance downstream for O_3 than NO and NO_2.

[46] We now turn to look at some of the secondary pollutants produced. To do this we use Mesh 2, which has a greater resolution particularly in the downstream direction. Much of the chemistry in the early plume is driven by the large amount of OH produced by combustion. Other 'fast' species, O, H, HO_2, NO_3, SO_3 and HSO_3 are produced very rapidly (within the first grid spacing). They then decay quickly within the first few meters of the jet. Further downstream they decay to levels lower than those in the background. Figure 7 shows the evolution in the first 10 m of three radicals (O, OH and SO_3), O shows the most rapid decay with OH slightly slower. SO_3 actually increases in the first part of the jet, although all three have been substantially consumed well before the end of the jet core at around 3 m. When the Stochastic Fields method is used we see a difference in the predicted evolution of these radicals from when segregation is ignored, this can be seen in Figure 8. There is some statistical noise here due to the use of relative few fields (twelve) and higher variance (cf. equation (11)). This could be improved by the use of more fields. However, the underlying trend here is clear and the integrated flow rate for the species shown in section 4.3, below, show good agreement between simulations using different random number sequences, also even if 18 fields were used instead of 12 the statistical error would only be reduced by less than 20%. After 2.5 m the Stochastic Fields and plain chemistry profiles for O and OH are very similar whereas for SO_3 the profile where segregation effects are included shows a reduced concentration. After 7.5 m O and OH levels with the plume have fallen to values lower than those in the background, the presence of segregation, however, appears to retard their decay within the plume. The SO_3 level has fallen in the center of the plume by 7.5 m leaving a region of increased concentration at the edge of the plume. Again, when we take into account segregation we see that this peak is reduced in height and moves toward the plume center and the concentration within the plume is increased. These differences are seen because the reactions involving these radicals at the edge of the plume are fast enough for the segregation to affect the reaction rate.

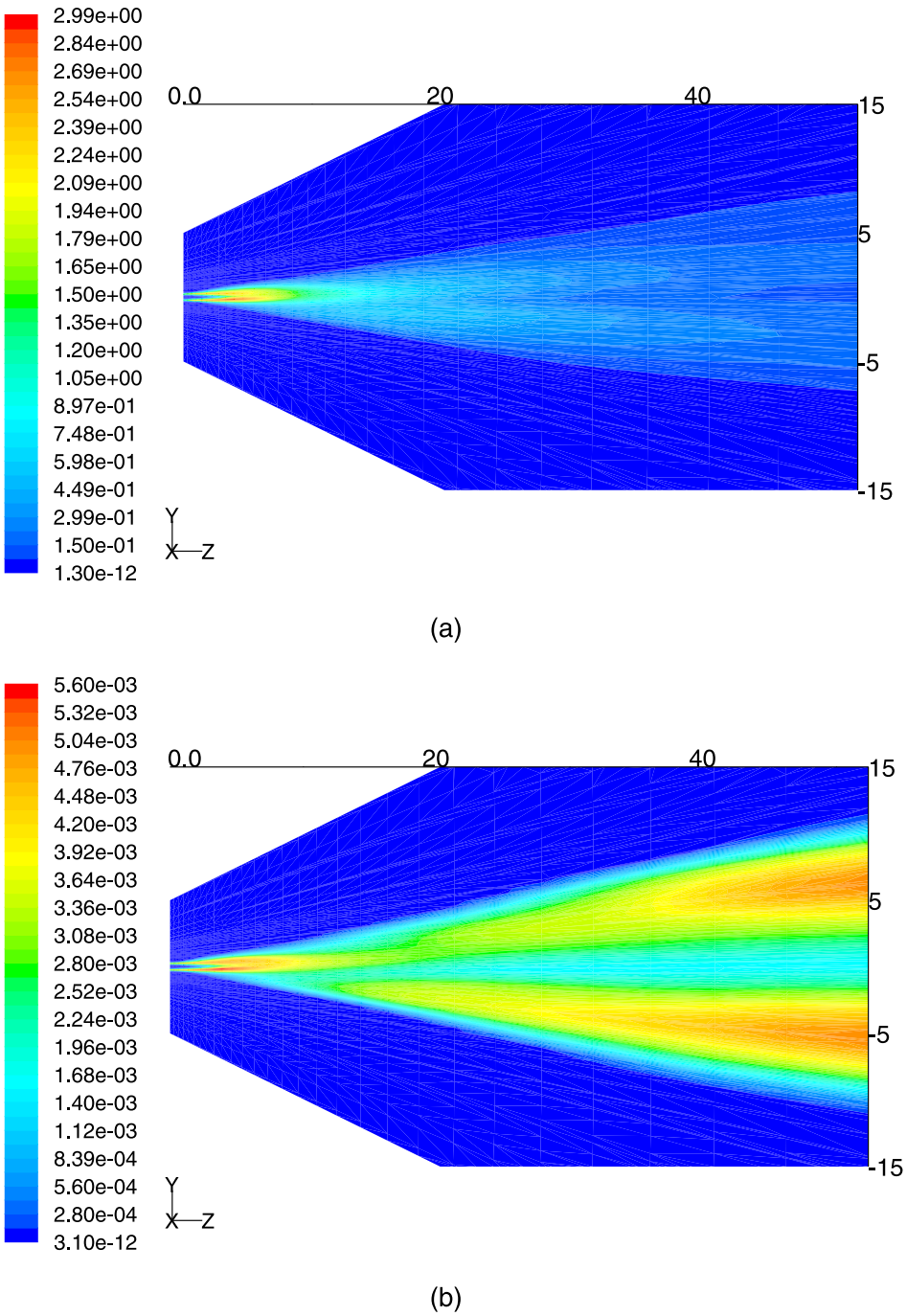

Figure 6. Contours of (a) *NO* and (b) O_3 RMS [ppm] on plane parallel with jet axis. Results from Stochastic Fields method for jet in still air.

[47] *Brown et al.* [1996] discuss the role of H_2SO_4 in aerosol production. This is formed from SO_2 in the exhaust via the intermediate species SO_3 and HSO_3. Figure 9 shows the evolution of H_2SO_4 along the center-line of the jet. We see that it is produced very rapidly; i.e., within the jet core before being mixed out by turbulent diffusion. Taking segregation into account has no discernable effect of the mean concentration, however the RMS fluctuations are of the order of 10% of the mean from the point where the turbulence reaches the center-line (3–4 m) onwards. Given the highly non-linear nature of the binary nucleation process [*Zhao and Turco*, 1995] these fluctuations in acid vapor concentration could have a significant effect on aerosol production.

[48] HNO_2 and HNO_3 are produced in the jet until a constant equilibrium level is reached which lasts until the end of the jet core. H_2O_2 is produced very rapidly, and would in fact be produced in the engine itself, it's concentration is reduced slightly by chemistry in the core before it is mixed out. Again we find that considering micromixing effects does not have a significant bearing on the predicted concentrations of these species. Figure 10 shows this along

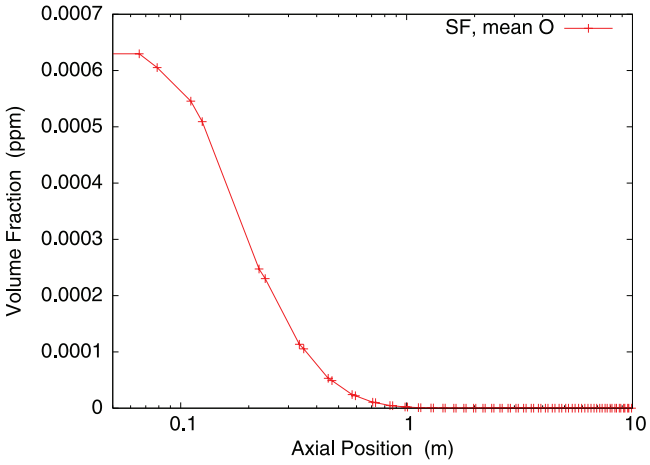

(a)

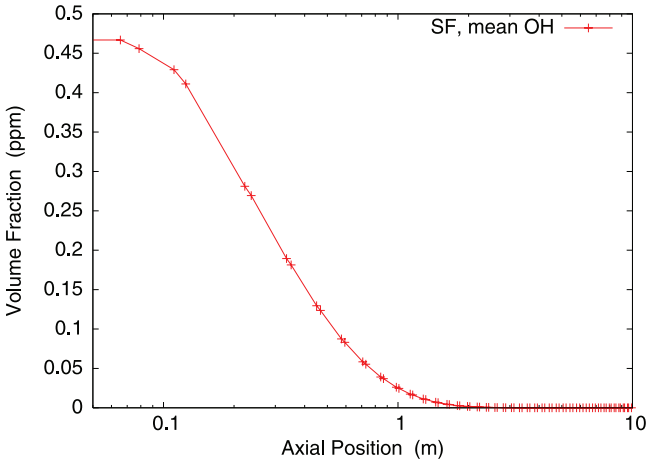

(b)

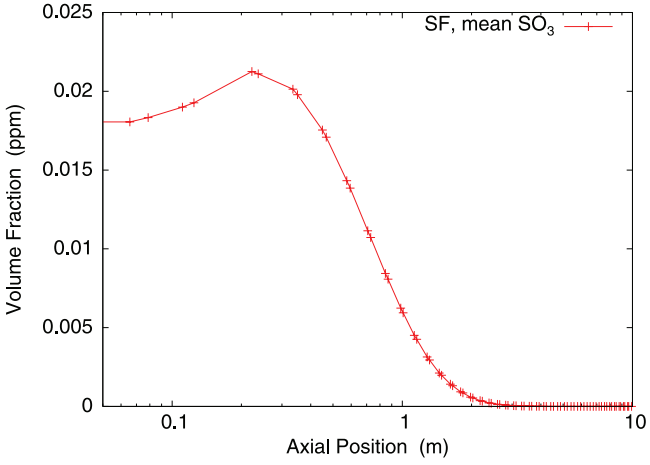

(c)

Figure 7. Axial evolution of (a) *O*, (b) *OH* and (c) SO_3 along center-line of jet into still air using Mesh 2. Calculations using Stochastic Fields model.

the center-line of the jet, the two predictions also agree in the radial direction as well, although this is not shown. This lack of segregation is most likely to be because most of the chemistry takes place early on within the plume rather than between species mixing from inside and outside of the plume [*Kärcher et al.*, 1996]. The exception to this is the NO-O_3 reaction discussed above. We have specified the inlet concentrations to be uniform across the jet. Because of this there are no gradients to cause segregation in the region where most of the reaction takes place. By the time the turbulence mixes into the jet the reaction has been nearly completed. If the concentration were not uniform in the jet, perhaps due to effects in the nozzle, then the effect of segregation may not be insignificant.

4.3. Damköhler Number

[49] As discussed in section 1 the parameter that characterizes the effect of segregation on reaction rate is the Damköhler number, *Da*. This is the ratio of a physical mixing timescale to a chemical timescale. A physical timescale has already been calculated in the CFD solution and is assumed to be the same for each species, this is shown in Figure 2b. An approximate method of obtaining a chemical timescale for each species is to find the rate at which it relaxes back to a local equilibrium value [*Neophytou et al.*, 2004]. We can split the reaction rate for species *i* into production and loss terms:

$$\frac{d\phi_i}{dt} = P_i - L_i\phi_i \tag{15}$$

[50] P_i and L_i are determined by the concentration of other species and the rate constants. If they are assumed to be constant and ϕ_i is perturbed, $\Delta\phi_i$, then it will relax back to its equilibrium level according to:

$$\Delta\phi_i \propto \exp(-L_i t) \tag{16}$$

[51] The timescale for species *i* is, therefore, $T_{chem} = 1/L_i$. The loss rates can easily be extracted from the CHEMEQ2 solver at each cell to give the distribution of timescale and hence $Da = T_{eddy}/T_{chem}$ can be calculated across the domain for each species. This is done for each field and the mean taken. Contour plots of mean *Da* for NO_2, O_3, SO_3, *OH* and *O* are shown in Figure 11.

[52] To investigate the influence of *Da* a quantitative measure of the effect of segregation on the different species is required. We use the total species flow rate through a plane perpendicular to the flow, $\dot{X}_i$, which is found by integration using FLUENT.

$$\dot{X}_i = \int X_i \rho \mathbf{v} \cdot d\mathbf{A} \tag{17}$$

[53] This was evaluated on planes perpendicular to the jet at 0.5 m, 2.5 m, 5.0 m and 7.5 m downstream of the jet using Mesh 2. This was done for the plain solution and three Stochastic Fields solutions using different random number sequences. The normalized difference between the plain and Stochastic fields solution was then found as $(\dot{X}_{SF} - \dot{X}_P)/\dot{X}_{SF}$. These results are shown in Table 2 for a selection of species.

[54] As noted earlier CO_2 is an inert species in the mechanism employed here and as such should be unaffected by the Stochastic fields method. Therefore we can use the normalized difference in flow rates for CO_2 as an approx-

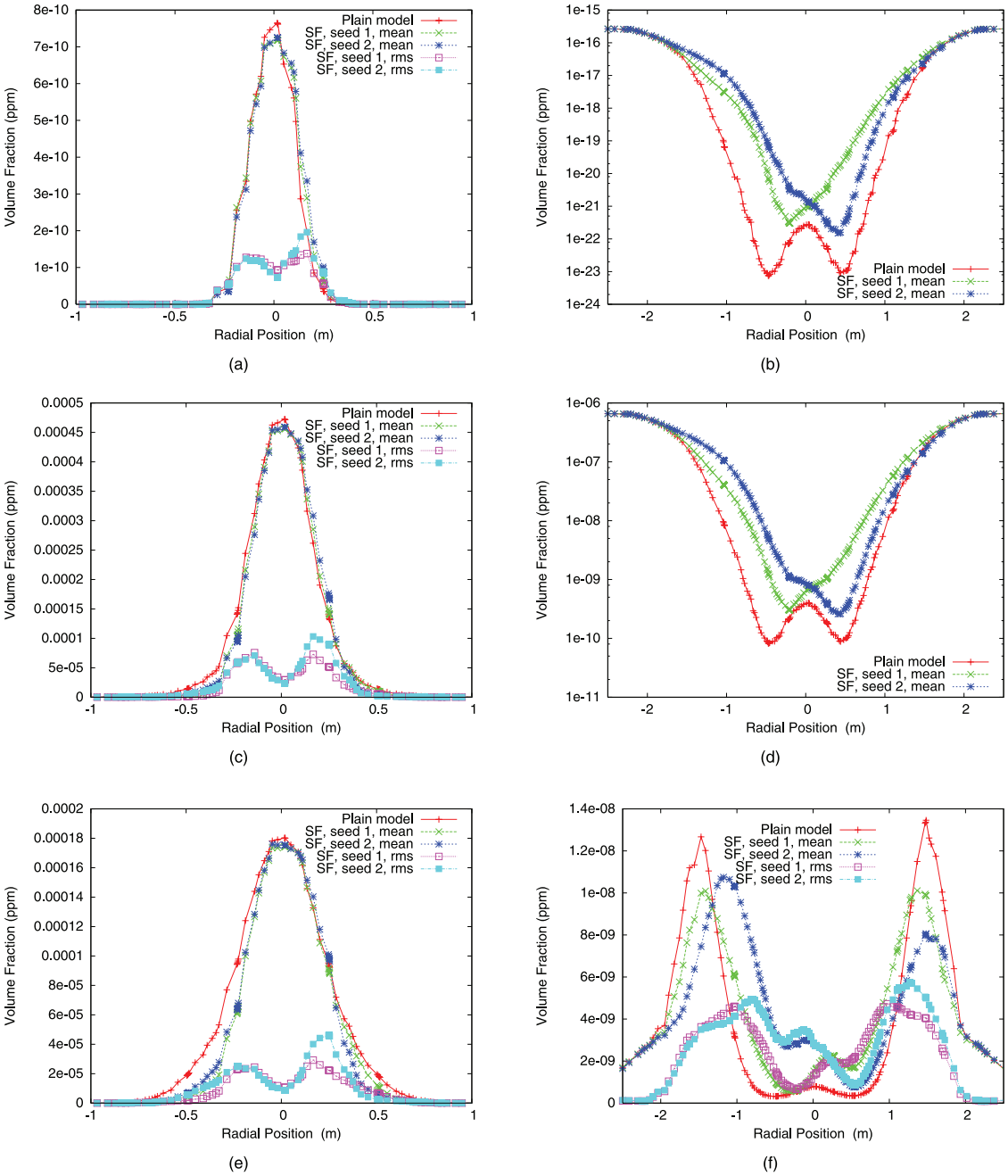

Figure 8. Radial profiles of *O*, *OH*, and SO_3 volume fraction mean and RMS by Stochastic Fields Method and simple advection-diffusion-reaction code. *O*, 2.5 m downstream (a); *O*, 7.5 m downstream (b); *OH*, 2.5 m downstream (c) and *OH*, 7.5 m downstream (d); SO_3, 2.5 m downstream (e) and SO_3, 7.5 m downstream (f). Results from Mesh 2, seed 1 and seed 2 refer to different random number sequences.

imate measure of the statistical uncertainty at that point. If we look at NO_2 and O_3 we see that at all four downstream positions the magnitude of the difference caused by considering segregation is of the same order as for CO_2, i.e., less than 2% for z = 7.5 m. This indicates that the difference is likely to be largely due to statistical error rather than micromixing effects. This supports the results seen in Figure 5. We might expect the reaction $NO + O_3 \rightarrow NO_2 + O_2$ to be affected by segregation, in this situation a plume of one reactant spreads into the other so that their gradients have the opposite sign and hence turbulence would be expected to lead to $\phi'_A\phi'_B$ taking a significant negative value, reducing the reaction rate [*Garmory et al.*, 2006]. However, Figures 11a and 11b show that *Da* is relatively low for these species (<1) other than in the core of the jet where it takes a value of around 20. Within the core there are no gradients and hence no segregation effects. For NO_2 *Da* rapidly drops to values of the order of 10^{-6}

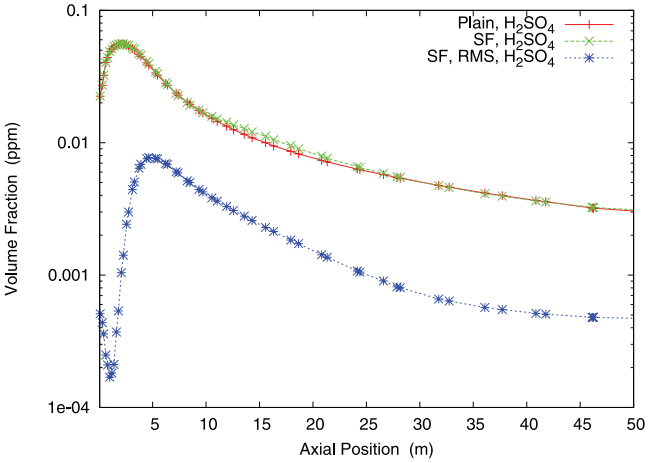

Figure 9. H_2SO_4 volume fraction along center-line of Mesh 1. Mean results from plain advection-diffusion-reaction code. Mean and RMS from Stochastic Fields.

indicating that the chemistry is much slower than the mixing for this species and hence reactant segregation does not have time to have an effect. For O_3 *Da* in the plume falls to a level of $O(10^{-1})$, while the chemistry is faster for O_3 than for NO_2, the chemistry is still not fast enough compared to the mixing for segregation to have an effect noticeable within the accuracy of this simulation.

[55] The result of ignoring segregation on the predicted levels of SO_3, *OH* and *O* are seen in Table 2 *O* has the largest *Da*, taking a minimum value of 60 (Figure 11e). This means that throughout the flow the chemistry will always be fast compared to the mixing and hence segregation will have an effect. This agrees with the results seen in Table 2 where the differences increase with downstream distance. These differences are significantly and consistently bigger than those for CO_2 hence we can be confident that this is due to segregation rather than statistical accuracy. The large increase between the difference at 2.5 m and 5.0 m is consistent with the turbulence reaching the center of the jet within this region. Figures 11c and 11d show that *Da* for *OH* and SO_3 are similar, taking values of the order of 10 in the early part of the plume. Again we see that for these species segregation has an effect. At 2.5 m the SO_3 flow rate is reduced by ~20% by segregation, but by 7.5 m it has been increased by ~40%. This is consistent with the results seen in Figure 8. SO_3 initially increases in the jet core before decaying (Figure 7c). This suggests that segregation may lead to slower radical chemistry when either producing or destroying radicals. The differences for SO_3, *OH* and *O* at 7.5 m do not show any trend with *Da*, this may be because of some other coupled effects in the mechanism or to the simplistic method we have used to calculate chemical timescales.

4.4. Discussion

[56] The Stochastic Fields method has been found to predict changed concentrations of fast decaying species around the edge of the jet core. This is the result of imperfect mixing at the microscale. For primary pollutants, such as NO_x, and secondary pollutants, such as HNO_2, the effects of micromixing are less significant. Dilution of the early plume by macromixing has a much greater effect on the dispersion and chemistry of the plume than the effect of imperfect mixing at the microscale. Work by *Wang and Chen* [1997] and *Menon and Wu* [1998] suggest that micromixing can effect NO_x and O_3 depletion by 1–2% over longer distances from the jet than studied here (up to 1000 jet diameters).

[57] Not included in this work are aerosol effects. *Brown et al.* [1996] discuss the important role of H_2SO_4 and its precursor SO_3 in the production of aerosols in an engine jet plume. In this work we have found that micromixing could have a significant effect on SO_3 levels in the plume. On the other hand it was found that the concentration of H_2SO_4 was unaffected. However, the fluctuations of acid vapor concentration, which were of the order of 10% of the mean, may have a significant effect on the highly non-linear nucleation process, particularly when coupled with temperature fluctuations.

[58] There are several advantages to coupling with a commercial CFD package. Setting up new cases and altering conditions is made easier by using the existing mesh building tools and user interfaces. Problems of exporting necessary data about the flow to the reacting flow code are avoided and the treatment of advection and diffusion is well established in the commercial code and does not need to be repeated. Finally, exporting and displaying data after the calculation is made easier. A disadvantage is that a fractional step method has to be used, there is no option to calculate all terms together. Here we have used the IEM model for micromixing, however future work could make use of alternative models [*Cassiani et al.*, 2005; *Fox*, 2003; *Soulard et al.*, 2004] that may be more difficult to implement in this coupled arrangement. A limit on the number of scalars that can be solved and the number of memory location at each cell in FLUENT would also provide difficulties if using more complex micromixing models as well as limiting the size of mechanism or number of fields.

[59] We have included some calculations of Damköhler number, which were calculated using the loss rate (see equation (15)) as the chemical timescale for each species.

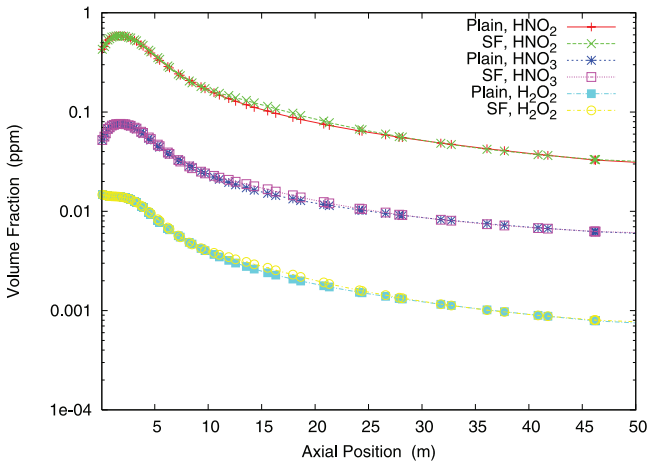

Figure 10. Evolution of HNO_2, HNO_3 and H_2O_2 along center-line of jet in Mesh 2 by both Stochastic Fields method and plain advection-diffusion-reaction method.

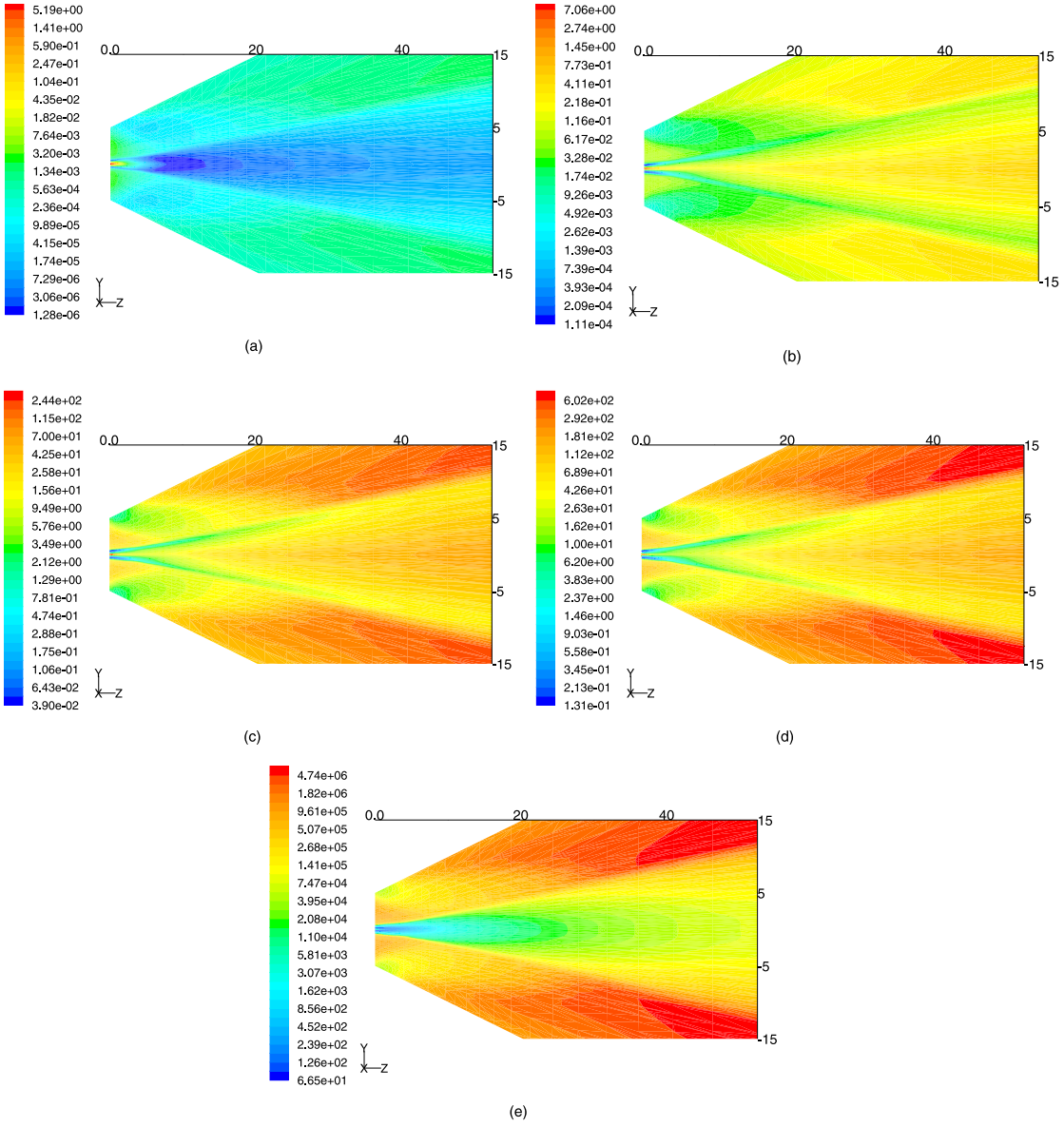

Figure 11. Contours of Damköhler number for (a) NO_2, (b) O_3, (c) SO_3, (d) OH and (e) O on a plane containing the jet axis using Mesh 1.

These rates appear as the diagonal elements of the Jacobian. A better method of finding chemical timescales is to find the eigenvalues of the Jacobian and associate each one with a particular species [*Neophytou et al.*, 2004]. The advantage of this is that it takes account of the effect of off diagonal elements on the timescale and will also provide a timescale for each species unlike the present method which gives no timescale for those species (e.g., H_2SO_4) that do not have loss terms in the mechanism.

5. Conclusions

[60] This work has used the Stochastic Fields or Field Monte Carlo method for turbulent reacting flows coupled with a commercial CFD package, FLUENT. This has been applied to a hot jet of Mach number 0.46 with a slower bypass jet, which approximated the conditions at the exhaust of a 100 kN turbofan engine at idle thrust setting. The reaction of pollutants in the early part of the jet are important when considering levels of pollution exposure and also aerosol production.

[61] For the 50 m section of the plume studied, the primary pollutant, NO, was little affected by chemistry in the plume. The concentration is so high compared to other species that its evolution is dominated by turbulent mixing, which occurs at the end of the jet core. Those species (OH, HO_2, O, H, SO_3, and HSO_3) which decay rapidly away from the jet exit plane do show a difference when micromixing is taken into account. A changed concentration of these radicals is found at the edge of the plume when the Stochastic Fields method is used. Subsequently an increase in volume fraction is seen across the plume at 7.5 m from the jet exit. These species are associated with relatively high Damköhler numbers. However, most of the chemistry with this mechanism takes place very early in the jet before the

Table 2. Normalised Difference Between Integrated Species Flow Rate (See Equation (17)) With and Without Segregation Effects at Axial Locations, z, Downstream of Jet

		Normalized Integrated Difference, %			
Z, m	Species	Seed 1	Seed 2	Seed 3	Mean
0.5	CO_2	−0.7	0.0	0.1	−0.2
	NO_2	−0.7	0.0	0.4	−0.1
	O_3	0.0	0.0	0.0	0.0
	SO_3	−1.0	−0.4	−3.2	−1.5
	OH	0.5	1.2	−3.7	−0.1
	O	7.1	7.9	−1.0	4.7
2.5	CO_2	1.6	1.5	−2.4	0.2
	NO_2	1.6	1.5	−2.0	0.3
	O_3	−0.2	−0.1	0.5	0.1
	SO_3	−22.4	−21.6	−20.0	−21.3
	OH	−8.0	−7.0	−8.6	−7.9
	O	9.6	10.0	5.9	8.5
5.0	CO_2	2.8	−1.6	−1.0	0.1
	NO_2	2.7	−1.3	−0.9	0.2
	O_3	−0.3	0.5	0.7	0.3
	SO_3	5.1	15.6	12.7	11.1
	OH	5.7	13.4	9.7	9.6
	O	23.0	34.3	20.4	25.9
7.5	CO_2	0.9	−5.6	−0.2	−1.6
	NO_2	0.9	−4.9	−0.2	−1.4
	O_3	0.1	1.9	1.1	1.0
	SO_3	30.2	47.7	35.8	37.9
	OH	25.6	36.6	28.8	30.4
	O	25.6	36.6	27.8	30.0

turbulence created in the shear layers diffuses into the jet *Kärcher et al.* [1996]. The chemistry producing secondary pollutants, such as H_2SO_4 or HNO_2, takes place in a region of low turbulence and uniform concentrations. Consequently we see that using the Stochastic Fields method does not always give significantly different results from a simple advection-diffusion-reaction model that does not take micromixing into account. Micromixing will only have an effect on reaction rates when there are temporal or spatial fluctuations in reactant concentration.

[62] The reaction between $NO + O_3 \rightarrow NO_2 + O_2$ is the only major reaction to take place between a species from inside the plume and one in the background and is, therefore, controlled by the mixing out of the plume. These are conditions in which micromixing could have an effect on the reaction rate, however there is no significant change in the region studied when the Stochastic Fields method is used. The Damköhler number has been found to be relatively low for O_3 and particularly NO_2, meaning that micromixing is fast compared to the chemistry so that reactant segregation is destroyed before it can alter the reaction rate. It was found that, for the flow inside the plume, there is a good correlation between the local Damköhler number and which species are affected by segregation. It was found that those species so affected were those for which Da took values greater than ∼5.

[63] **Acknowledgments.** This work has been funded by the EPSRC. REB acknowledges support from NERC and the Institute for Aviation and the Environment, Cambridge. AG acknowledges a Scholarship from The Leathersellers' Company.

References

Brown, R. J., and R. W. Bilger (1998), Experiments on a reacting plume-1. Conventional concentration statistics, *Atmos. Environ.*, *32*, 611–628.

Brown, R. C., R. C. Miake-Lye, M. R. Anderson, C. E. Kolb, and T. J. Resch (1996), Aerosol dynamics in near-field aircraft plumes, *J. Geophys. Res.*, *101*(D17), 22,939–22,953.

Byrne, G. D. (1992), Pragmatic experiments with Krylov methods in the stiff ODE setting, in *Computational Ordinary Differential Equations*, edited by J. Cash and I. Gladwell, Oxford University Press.

Cassiani, M., P. Franzese, and U. Giostra (2005), A PDF micromixing model of dispersion for atmospheric flow. Part i: Development of the model, application to homogeneous turbulence and to neutral boundary layer, *Atmos. Environ.*, *39*, 1457–1469.

Cha, C. M., and P. Trouillet (2003), A model for the mixing time scale of a turbulent reacting scalar, *Phys. Fluids*, *15*, 1375–1380.

Department For Transport (2003), *The Future of Air Transport*, HM Stationary Office.

Dopazo, C. (1975), Probability density function approach for an axisymmetric heated jet: Centreline evolution, *Phys. Fluids*, *18*, 397.

Fox, R. O. (2003), *Computational Models for Turbulent Reacting Flows*, Cambridge University Press, Cambridge.

Galmarini, S., J. Vilà-Guerau de Arellano, and P. G. Duynkerke (1995), The effect of microscale turbulence on the reaction rate in a chemically reactive plume, *Atmos. Environ.*, *29*(1), 87–95.

Gardiner, C. W. (2004), *Handbook of Stochastic Methods*, 3rd ed., Springer, Berlin.

Garmory, A., E. S. Richardson, and E. Mastorakos (2006), Micromixing effects in a reacting flow by the Stochastic fields method, *Atmos. Environ.*, *40*, 1078–1091.

Greener By Design (2005), *Mitigating the Environmental Impact of Aviation: Opportunities and Priorities*, Royal Aeronautical Society.

Herndon, S. C., et al. (2004), *NO* and NO_2 emission ratios measured from in-use commercial aircraft during taxi and takeoff, *Environ. Sci. Technol.*, *38*, 6078–6084.

Hilst, G. R. (2000), Segregation and chemical reaction rates in air quality models, *Atmos. Environ.*, *32*, 3891–3895.

ICAO (2004), Engine exhaust emissions data bank, V2525-D5, Unique ID 1IA002.

Jacobson, M. Z. (1999), *Fundamentals of Atmospheric Modeling*, Cambridge University Press, Cambridge.

Jones, W. P., and M. Kakhi (1998), PDF modelling of finite-rate chemistry effects in turbulent nonpremixed jet flames, *Combust. Flame*, *115*, 210–229.

Kärcher, B., M. M. Hirschberg, and P. Fabian (1996), Small-scale chemical evolution of aircraft exhaust species at cruising altitudes, *J. Geophys. Res.*, *101*(D10), 15,169–15,190.

Kloeden, P. E., and E. Platen (1999), *Numerical Solution of Stochastic Differential Equations*, Springer, Berlin, corrected third printing edition.

Laso, M., and H. C. Öttinger (1993), Calculation of viscoelastic flow using molecular models: The Connffessit approach, *J. Non Newtonian Fluid Mech.*, *47*, 1–20.

Lewellen, D. C., and W. S. Lewellen (2001), Effect of aircraft wake dynamics on measured and simulated NO_x and HO_x wake chemistry, *J. Geophys. Res.*, *106*(D21), 27,661–27,672.

Liang, J., and M. Z. Jacobson (2000), Effects of subgrid segregation on ozone production efficiency in a chemical model, *Atmos. Environ.*, *34*, 2975–2982.

Menon, S., and J. Wu (1998), Effects of micro- and macroscale turbulent mixing on the chemical processes in engine exhaust plumes, *J. Appl. Meteorol.*, *37*, 639–654.

Mott, D. R., and E. S. Oran (2001), Chemeq2: A solver for stiff ordinary equations of chemical kinetics, *Naval Research Laboratory*, Technical Report 8553.

Mustata, R., L. Valiño, C. Jiménez, W. P. Jones, and S. Bondi (2006), A probability density function eulerian Monte Carlo field method for large-eddy simulations, Application to a turbulent piloted methane/air diffusion flame (Sandia D), *Combust. Flame*, *145*, 88–104.

Neophytou, M., D. A. Goussis, M. van Loon, and E. Mastorakos (2004), Reduced chemical mechanisms for atmospheric pollution using computational singular perturbation analysis, *Atmos. Environ.*, *38*, 3661–3673.

Oran, E. S., and J. P. Boris (2001), *Numerical Simulation of Reactive Flow*, 2nd ed., Cambridge University Press, Cambridge.

Richards, C. D., and W. M. Pitts (1993), Global density effects on the self-preservation behavior of turbulent free jets, *J. Fluid Mech.*, *254*, 417–435.

Sabel'nikov, V., and O. Soulard (2005), Rapidly decorrelating velocity-field model as a tool for solving one-point Fokker-Planck equations for probability density functions of turbulent reactive scalars, *Phys. Rev. E*, *72*(1), 016301.

Sabel'nikov, V., and O. Soulard (2006), White in time scalar advection model as a tool for solving joint composition PDF equations, *Flow Turbul. Combust.*, *77*, 333–357.

Soulard, O., V. Sabel'nikov, and M. Gorokhovski (2004), Stochastic scalar mixing models accounting for turbulent frequency multiscale fluctuations, *Int. J. Heat Fluid Flow*, *25*, 875–883.

Spalding, D. B. (1995), Multi-fluid models of turbulent combustion, in *CTAC95 Conference*, Melbourne, Australia.

Tennekes, H., and J. L. Lumley (1972), *A First Course in Turbulence*, MIT Press, Massachusetts.

Treviño, C., and F. Méndez (1999), Simplified model for the prediction of ozone generation in polluted urban areas with continuous precursor species emissions, *Atmos. Environ.*, *33*, 1103–1110.

Valiño, L. (1998), A field Monte Carlo formulation for calculating the probability density function of a single scalar in a turbulent flow, *Flow Turbul. Combust.*, *60*, 157–172.

Vilà-Guerau de Arellano, J., A. Dosio, J.-F. Vinuesa, A. A. M. Holtslag, and S. Galmarini (2004), The dispersion of chemically reactive species in the atmospheric boundary layer, *Meteorol. Atmos. Phys.*, *87*, 23–38.

Vinuesa, J.-F., and J. Vilà-Guerau de Arellano (2003), Fluxes and (co-)variances of reacting scalars in the convective boundary layer, *Tellus B*, *55*(4), 935–949.

Wang, Z., and J. Y. Chen (1997), Modeling of microscale turbulence and chemistry interaction in near-field aircraft plumes, *J. Geophys. Res.*, *102*(D11), 12,871–12,883.

Zhao, J., and R. P. Turco (1995), Nucleation simulations in the wake of a jet aircraft in stratospheric flight, *J. Aerosol Sci.*, *26*(5), 779–795.

R. E. Britter, A. Garmory, and E. Mastorakos, Department of Engineering, University of Cambridge, Trumpington Street, Cambridge, CB2 1PZ, UK. (ag310@cam.ac.uk)